Crossed-Beam Reactions of Barium with Hydrogen Halides

Measurement of Internal State Distributions by Laser-Induced Fluorescence

By H. W. Cruse, P. J. Dagdigian and R. N. Zare

Department of Chemistry, Columbia University, New York, New York 10027, U.S.A.

Received 22nd January, 1973

The use of laser-induced fluorescence as a molecular beam detector for the measurement of internal state distributions of reaction products is presented and applied to the reactions of barium with the hydrogen halides. It is found that most of the reaction exoergicity appears as translational energy of the products and that the total reactive cross section is positively correlated with the average fraction of the exoergicity appearing as vibrational excitation.

Conventional molecular beam reactive scattering studies have excelled in the determination of the angular and velocity distributions of reaction products, but direct information on the internal state distributions has been sparse.[1] One of the most important of the non-beam methods for learning about the partitioning of reaction energy into the internal degrees of freedom of the products has been infra-red chemiluminescence studies.[2] Unfortunately, this technique has hitherto been limited to hydride compounds, principally hydrogen halides. We present an alternative technique based on electronic fluorescence spectroscopy.

In this method, a tunable narrow-band light source is swept in wavelength. When it coincides with a molecular absorption line, the molecule makes a transition to an excited electronic state and is detected by observing the subsequent light emission of the molecule. One of the principal advantages of this technique is its specificity, for it is possible to identify unequivocally the absorbing molecule and to assign internal quantum numbers. Moreover, the sensitivity of electronic fluorescence detection using presently available tunable laser sources appears to exceed that of a universal ionizer.

In this paper we describe the use of laser-induced fluorescence as a molecular beam detector and apply it to the reactions of barium atoms with hydrogen halides,

$$\mathrm{Ba}+\mathrm{HX}\rightarrow\mathrm{BaX}(X^2\Sigma^+)+\mathrm{H};\ \mathrm{X}=\mathrm{F, Cl, Br, I.} \qquad (1\text{-}4)$$

Reactions (1)-(3) have not been studied using beam techniques; however, an angular distribution has been measured for reaction (4).[3] We report the vibrational population distributions of the BaX products, approximate rotational distributions in reactions (1) and (2), and relative total reactive cross sections for the four reactions.

EXPERIMENTAL

The experimental arrangement consists of a simple molecular beam apparatus, a pulsed tunable dye laser for exciting fluorescence, and a gated optical detection system.

MOLECULAR BEAM SYSTEM

The beam apparatus is housed inside a cylindrical stainless steel chamber (70 cm long and 25 cm diam.) that is evacuated by two 4-inch diffusion pumps (effective pumping speed

700 l. s^{-1}). A metal atom beam and a gas beam intersect to form the reaction zone through which the laser beam is directed (see fig. 1). The laser-induced fluorescence is viewed at right angles to the laser beam by a photomultiplier. In some experiments, the hydrogen halide beam source is replaced by a gas jet so that the vacuum chamber serves essentially as a scattering box, as in earlier preliminary experiments.[4]

The barium atom beam effuses from a molybdenum oven (orifice diam. 0.3 cm) that is resistively heated to between 1000 and 1100 K using tantalum wire windings. The oven is

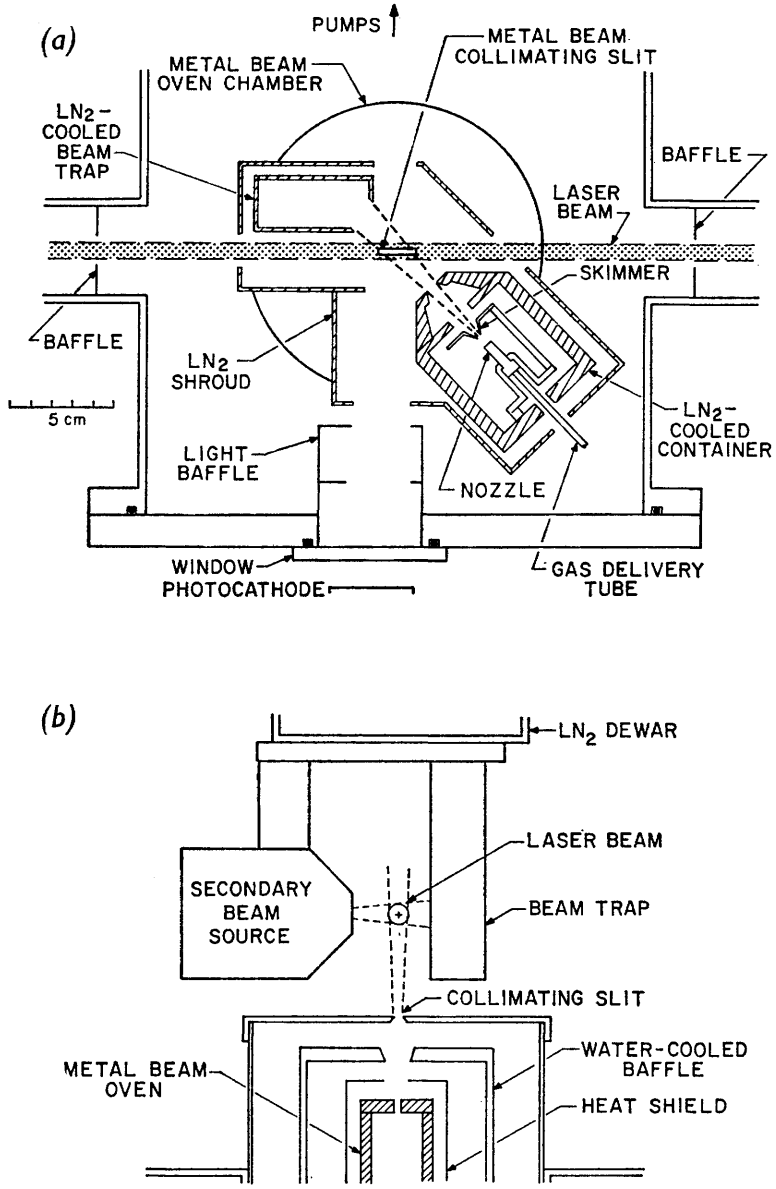

FIG. 1.—The molecular beam apparatus: (*a*) top view, (*b*) side view. In (*b*) the laser beam is perpendicular to the plane of the figure and the secondary beam source has been rotated by 45° about the Ba beam axis for clarity.

situated beneath the main vacuum chamber in a separate chamber evacuated by another 4-inch diffusion pump. The barium beam passes into the main chamber through a rectangular slit, 0.2×1.9 cm in size, located 4 cm from the oven orifice. When the gas beam source is used, the collimating slit is 5 cm below the reaction zone through which the laser beam passes. With the scattering box arrangement, the slit is 2.5 cm below the laser beam. The metal beam flux is measured using a film thickness monitor (Granville–Phillips) and is typically 2×10^{15} atom cm^{-2} s^{-1}, corresponding to a density in the reaction zone of 5×10^{10} atom cm^{-3}.

The hydrogen halide beam source consists of a stainless steel nozzle (orifice diam. 0.025 cm) with a conical-shaped stainless steel skimmer, 0.13 cm diam. and 0.5 cm from the nozzle. The nozzle and skimmer assembly is surrounded by a liquid-nitrogen-cooled copper shroud. A Nichrome heater is used to maintain the nozzle and skimmer assembly near room temperature. Final collimation of the beam is provided by a 0.60 cm diam. hole in the copper shroud. The beam angular divergence is about 10° FWHM. After traversing the reaction zone, the hydrogen halide beam enters a liquid-nitrogen-cooled " catcher ". Both the beam source and beam catcher are suspended from a liquid nitrogen dewar situated directly above the barium oven. Additional liquid-nitrogen-cooled copper shields partially surround the beam source and catcher (see fig. 1) to reduce heating by room-temperature black-body radiation. In addition, the shielding serves to reduce extraneous scattered light from the oven and from the laser beam. The hydrogen halide source is normally operated at 20 Torr and the calculated beam density in the reaction zone is 6×10^{11} molecule cm^{-3}. Note that the laser beam passes through the long axis of the reaction zone in order to maximize the absorption path length.

With both molecular beams in operation, the pressure in the main chamber is 1×10^{-6} Torr. The maximum rise in pressure due to the secondary beam source is 3×10^{-7} Torr for HCl, while for the other gases it is 1×10^{-7} Torr or less. For the scattering box arrangement with a pressure of 2×10^{-5} Torr of reactant gas in the main chamber, the pressure in the oven chamber is 3×10^{-6} Torr of which 1×10^{-6} Torr is attributable to the reactant gas. The quoted pressures are uncorrected ionization gauge measurements.

All hydrogen halide samples are purified before use: HCl, HBr, HI (Matheson Gas Products), and DCl (Merck) are condensed at 77 K, pumped on, and then distilled to remove parent halogen impurities; HF (Matheson), which is handled in a copper vacuum line fitted with Monel valves, is condensed at 196 K and pumped on to remove SiF_4.[5]

FLUORESCENCE EXCITATION AND DETECTION

The internal state distributions of the barium halide reaction products are determined by monitoring the fluorescence intensity as a function of excitation wavelength. Fig. 2 shows a block diagram of the tunable dye laser and fluorescence detection equipment. A pulsed nitrogen laser (Avco–Everett Research Laboratories) is used to pump a noncirculating dye solution contained in a closed cell. The dye laser cavity is formed by a 50 % reflecting (output) mirror and a 600 groove mm^{-1} diffraction grating (Bausch and Lomb) used in 5th order to select the desired laser wavelength. An intra-cavity 20 power beam expander narrows the bandwidth of the laser beam.[6] The dyes 3-aminophthalimide and brilliant sulphaflavine (saturated solutions in ethanol) cover the required wavelength range in two steps: 485-530 and 515-565 nm. The energy output of the dye laser is typically 10^{-5} J per pulse, corresponding to 3×10^{13} photons per pulse. The duration of a pulse is about 5 ns and the repetition rate is 10 pps.

The laser beam passes through a double polarizer that both selects the polarization of the light source (usually perpendicular to the barium beam) and serves as a convenient and continuous method for attenuating the laser intensity. The beam then passes into the main vacuum chamber through a 40 cm focal length lens sealed to the end of a 60 cm long side arm. This lens collimates the slightly divergent laser beam, which at the reaction zone is about 1 cm diam. The laser beam exits from the vacuum chamber through a window also sealed to the end of a sidearm.

During an experimental run, the laser wavelength is scanned by a variable-speed clock

motor (Erwin Halstrup, Kirchzarten, West Germany) connected to the grating tilt control, and the laser intensity is monitored continuously using a photodiode combined with a gated amplifier or is monitored at approximately 1 nm intervals by a 1 m spectrometer (Interactive Technology) that provides laser wavelength and bandwidth data. The laser bandwidth is typically 0.05 nm and the variation in the laser wavelength at a fixed grating setting is not detectable (<0.005 nm), while under the same conditions the variation in the laser intensity is less than 5 % over a 10 min period (detector output time constant of 3 s, corresponding to 30 pulses).

An RCA 7265 photomultiplier (S-20 photocathode) detects the reaction product fluorescence. The photomultiplier is located 15 cm from the reaction zone behind a quartz window in the main chamber. Only 0.5 % of the fluorescence impinges on the photocathode which has a quantum efficiency of about 20 %. Thus, at best only one laser-excited molecule in a thousand is detected. Following the short excitation pulse, the intensity of the molecular fluorescence decays exponentially with a lifetime which is characteristic of the excited state.

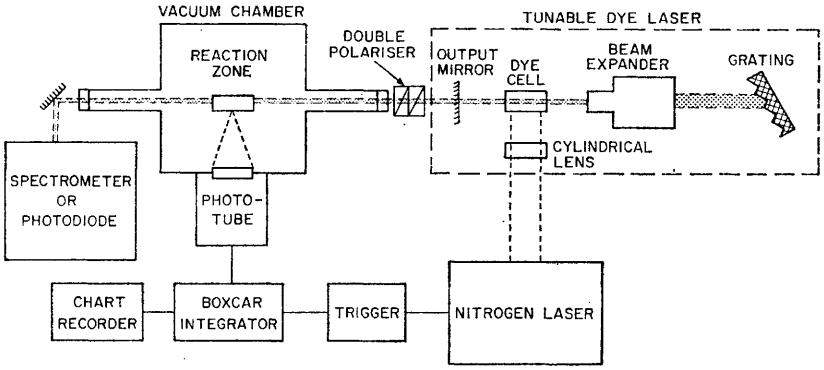

FIG. 2.—Schematic of the tunable dye laser and fluorescence detection equipment.

The photomultiplier output is detected, therefore, either by a fast oscilloscope (Tektronix model 454 or 7904) or by a boxcar integrator (Keithley Instruments models 881 and 882). The latter device (1) operates as a gated amplifier, detecting that signal appearing during and immediately after the laser pulse, and (2) averages the signals associated with many laser pulses. In these experiments, where the product molecule excited-state lifetimes are all approximately 15 ns,[7] a gate width of 100 ns is used.

In previous experiments, unwanted scattered light, which can be many times more intense than the desired fluorescence signal, was removed either by delaying the opening of the boxcar gate or by using a cutoff filter at the laser wavelength.[4] However, these remedies are not well suited to the present experiment because (1) the product molecule radiative lifetimes are comparable to the laser pulse duration and the discrimination time of the detection electronics and (2) most fluorescence occurs at wavelengths close to the laser line. Instead, carefully aligned baffles (shown in part in fig. 1) are placed in the long sidearms and in front of the photomultiplier and the interior of the main chamber is blackened with Nextel paint (3M Company). In this manner the scattered light level is reduced to the equivalent of about one photoelectron per pulse.

RESULTS

The BaX reaction products are detected by observing the laser-induced fluorescence of the $C^2\Pi$–$X^2\Sigma^+$ band systems that lie near 500 nm. Fig. 3-6 present typical scans showing the variation of fluorescence intensity with excitation wavelength. The scan rates are between 0.1 and 0.5 nm min^{-1}, the detector time constant being 1 s. The variation of laser intensity with wavelength is small for all these scans (<10 %). Within experimental error identical results are obtained using the second-

ary beam source and scattering chamber arrangements, the latter operating at HX gas pressures of $1\text{-}2\times10^{-5}$ Torr. Since no discernible alteration of the fluorescence spectra occurs upon increasing (or decreasing) the HX pressure by a factor of four, we conclude that rotational or vibrational collisional relaxation is negligible under the conditions used. The data are also unaffected by vibrational radiative decay since we estimate that the vibrational lifetimes, for all levels observed in these experiments, are larger by more than two orders of magnitude than the time delay between product formation and detection ($<10^{-4}$ s).

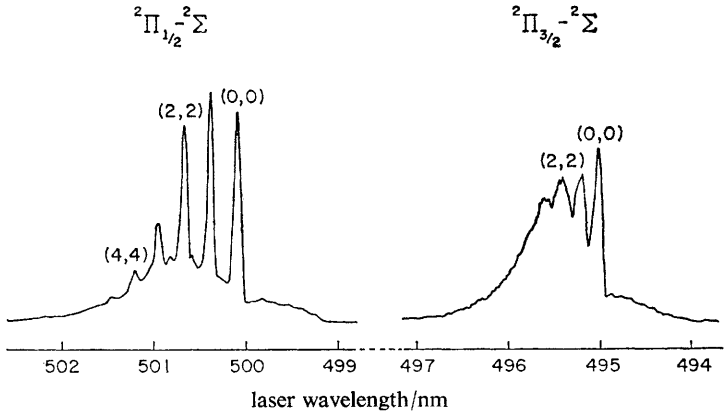

FIG. 3.—Variation of BaF fluorescence intensity with laser wavelength for the reaction Ba+HF→BaF+H. The band heads of the BaF $C^2\Pi$–$X^2\Sigma^+$ system are designated by (v', v'').

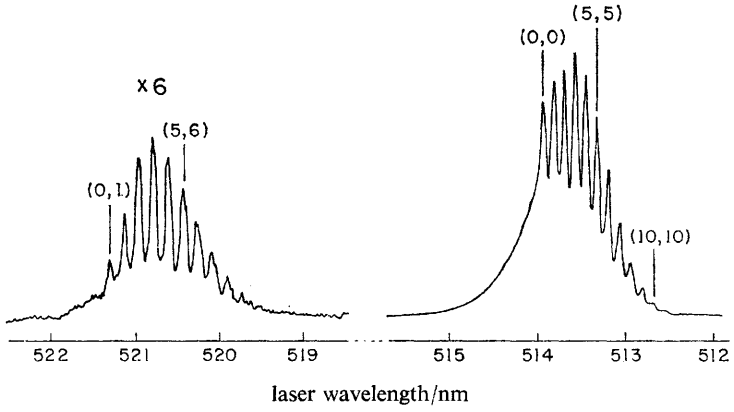

FIG. 4.—Variation of BaCl fluorescence intensity with laser wavelength for the Ba+HCl→BaCl+H reaction. The $C^2\Pi_{\frac{3}{2}}$–$X^2\Sigma^+$ $\Delta v = 0$ and -1 sequences are shown, the latter with a 6 times more sensitive ordinate scale.

The outstanding features of these band systems are the small spacing between the bands of a vibrational sequence and the dominant intensity of the $\Delta v = 0$ (diagonal) sequence. These facts indicate that the potential curves for the C and X states are nearly identical and help to explain why no rotational analysis has been carried out in the spectroscopic studies of these BaX band systems.[8-12] In order to extract meaningful internal state populations from the data shown in fig. 3-6, it is necessary to

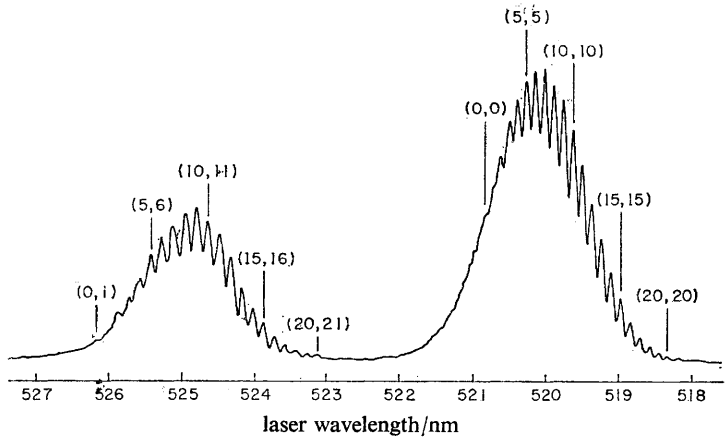

FIG. 5.—Variation of BaBr fluorescence intensity with laser wavelength for the Ba+HBr→BaBr+H reaction. The $C^2\Pi_{\frac{3}{2}}$–$X^2\Sigma^+$ $\Delta v = 0$ and -1 sequences are shown.

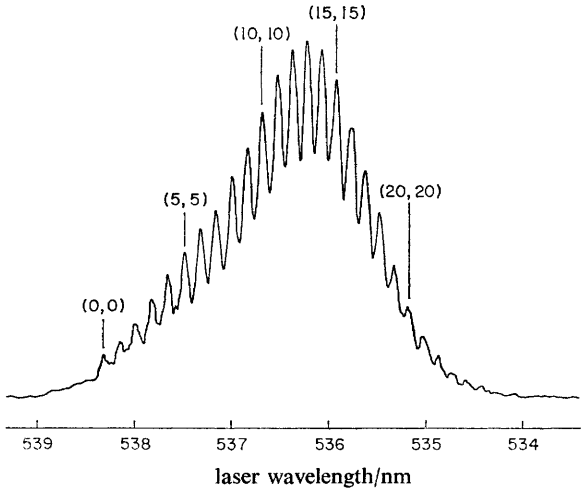

FIG. 6.—Variation of BaI fluorescence intensity with laser wavelength for the Ba+HI→BaI+H reaction. The $C^2\Pi_{\frac{3}{2}}$–$X^2\Sigma^+$ $\Delta v = 0$ sequence is shown.

estimate the molecular constants characterizing these band systems so that the formation of the band heads can be interpreted and the intensity of the bands can be related to the internal state populations through calculated Franck–Condon factor arrays.

ESTIMATES OF MOLECULAR CONSTANTS FOR THE BaX $C^2\Pi$–$X^2\Sigma^+$ BAND SYSTEMS

For a $^2\Pi$–$^2\Sigma^+$ transition there are a total of 12 branches whose members have line positions given by

$$F_i(J') - F_j(N'') = \nu_0^{(i)} + B_{\text{eff}}^{(i)} J'(J'+1) - B''N''(N''+1) \qquad (1)$$

where $i = 1$ or 2 denotes the $^2\Pi_{\frac{1}{2}}$ or $^2\Pi_{\frac{3}{2}}$ fine structure components of the $C^2\Pi$ state and $j = 1$ or 2 denotes the $J'' = N'' + \frac{1}{2}$ and $J'' = N'' - \frac{1}{2}$ spin components of the

$X^2\Sigma^+$ state. In eqn (1) centrifugal distortion corrections, Λ doubling in the upper state and spin splitting in the lower state have been disregarded. Here $\nu_0^{(i)}$ is the band origin of the $^2\Pi_i$–$^2\Sigma^+$ subband and $B_{\text{eff}}^{(i)}$ is an effective rotational constant that is related to the mechanical rotational constant B_v by $B_{\text{eff}}^{(i)} = B_v + (-1)^i B_v^2/A_v$, for $A_v \gg B_v$, where A_v is the spin-orbit constant (assumed to be positive [13]). Because of the spin-orbit splitting in the C state, each (v', v'') band shows four band heads. Since the bands are degraded to the red, the band heads are formed by the $Q_1 + R_{12}$ and R_1 branches in the $^2\Pi_{\frac{1}{2}}$–$^2\Sigma^+$ subband and by the $R_2 + Q_{21}$ and R_{21} branches in the $^2\Pi_{\frac{3}{2}}$–$^2\Sigma^+$ subband.[14]

The molecular constants for the C–X system are obtained by assuming that the C and X states are described by Morse oscillators for the low-lying vibrational levels. Then the vibrational spacings are exactly represented by $G(v) = \omega_e(v+\frac{1}{2}) - \omega_e x_e(v+\frac{1}{2})^2$ and the rotational constant α_e may be found from a knowledge of B_e, ω_e and $\omega_e x_e$.[15]

For BaF, the rotational constant B_0'' is known from an analysis of other band systems,[16] which together with approximate values of ω_e'' and $\omega_e x_e''$ permit the determination of α_e''. Values of $B_{\text{eff}}^{(i)}$ are then obtained from eqn (1) by using the separation between the two heads of each (v', v'') subband measured by Jenkins and Harvey.[8] The errors introduced into $B_{\text{eff}}^{(i)}$ by using band head separations should be small since the separation of the band heads is large compared to their experimental uncertainties. The $B_{\text{eff}}^{(i)}$ values are found to differ from the B'' values by only 1 %. The band origins, $\nu_0^{(i)}$, are then obtained from the measured band head positions using the B'' and $B_{\text{eff}}^{(i)}$ values. The rotational constant B_e' is obtained by averaging the $B_{\text{eff}}^{(i)}$ values. Finally, a linear least squares fit is made to these derived band origins to obtain vibrational constants for both states. In this last step, ω_e' and $\omega_e x_e'$ are forced to be the same for both subbands by allowing A_v to vary linearly with $(v+\frac{1}{2})$, i.e., $A_v = A_e + a_e(v+\frac{1}{2})$. The spectroscopic constants found in this manner for BaF are listed in table 1.

TABLE 1.—ESTIMATED SPECTROSCOPIC CONSTANTS (cm^{-1}) OF THE BARIUM MONOHALIDE $C^2\Pi$–$X^2\Sigma^+$ BAND SYSTEMS

		BaF	BaCl	BaBr	BaI
$X^2\Sigma^+$	ω_e''	469.26(9)	279.92(10)	189.3(20)	163.0(2)
	$\omega_e x_e''$	1.822(1)	0.785(3)	0.22(5)	0.42(1)
	B_e''	0.216 44	0.080 78		
	α_e''	0.001 17	0.000 33		
$C^2\Pi$	ω_e'	459.32(9)	283.08(10)	193.5(20)	168.7(2)
	$\omega_e x_e'$	1.679(1)	0.772(3)	0.19(5)	0.43(1)
	B_e'	0.214 28	0.079 77		
	α_e'	0.001 22	0.000 34		
	$T_{00}(^2\Pi_{\frac{1}{2}})$	19 987.7	19 062.5	18 651	17 816.2
	$B_{\text{eff}}^{(1)}(v = -\frac{1}{2})$	0.213 79	0.079 57		
	$T_{00}(^2\Pi_{\frac{3}{2}})$	20 185.7	19 451.6	19 193	18 571.5
	$B_{\text{eff}}^{(2)}(v = -\frac{1}{2})$	0.214 77	0.079 97		
	A_e	195.6(2)	387.6(3)	542.1(20)	755.3(25)
	a_e	4.74(3)	2.87(3)	1.50(6)	0.1(6)

The numbers in parenthesis are 3σ of the fit in units of the last quoted digit.

A similar analysis is carried out for BaCl, whose band head separations have been measured by Parker.[9] The B_e'' value is estimated from electron diffraction data on $BaCl_2$ using the empirical observation [18] that the bond length of an alkaline earth

monohalide is approximately 3 % smaller than that of the dihalide. The spectroscopic constants obtained for BaCl are also listed in table 1.

The spectroscopic data presently available for BaBr [10, 11] and BaI [12] preclude a similar treatment. Only single band heads have been reported in the case of BaI, while for BaBr the errors in the band head separations reported by Harrington [11] are deemed too large for the calculation of reliable Franck–Condon factors. The vibrational constants describing the band heads are also included in table 1. The single heads reported by Hedfeld [10] are used for BaBr. In the case of BaI, the ground state parameters are obtained from a fit to the $D^2\Sigma^+$–$X^2\Sigma^+$ band heads reported by Reddy and Rao,[19] while the upper state parameters are derived from a fit to the reported band heads of the C–X $\Delta v = 0$ sequence.[12]

Morse Franck–Condon factors are numerically calculated for BaF and BaCl by standard means. The results for BaF and BaCl are listed in table 2. For BaF the $\Delta v = 0$ sequence is by far the strongest and the three sequences $\Delta v = 0, \pm 1$ account for a minimum of 99 % of the $q_{v'v''}$ sum for v'' values up to 9. For BaCl the $\Delta v = \pm 1$ sequences become more important as v'' increases. It can be seen that even for the highest v'' value listed ($v'' = 9$), the sum of the $q_{v'v''}$ for the three sequences $\Delta v = 0, \pm 1$ is about 94 %. It is to be emphasized that the Franck–Condon factors depend much more sensitively on the difference $B'_v - B''_v$ than on the absolute values of B'_v and B''_v. Thus the calculational procedure described above is expected to give fairly reliable Franck–Condon factors for the $\Delta v = 0$ sequence even if the absolute values of B'_v and B''_v values are somewhat uncertain.

TABLE 2.—FRANCK–CONDON FACTORS CALCULATED FROM THE SPECTROSCOPIC CONSTANTS OF TABLE 1

v''	$v' = v''-1$	$v' = v''$	$v' = v''+1$
		BaF $C^2\Pi$–$X^2\Sigma^+$	
0		0.9868	0.0130
1	0.0131	0.9614	0.0251
2	0.0255	0.9375	0.0362
3	0.0371	0.9151	0.0464
4	0.0479	0.8943	0.0557
5	0.0581	0.8749	0.0642
6	0.0675	0.8568	0.0718
7	0.0764	0.8401	0.0788
8	0.0846	0.8247	0.0849
9	0.0923	0.8105	0.0904
		BaCl $C^2\Pi$–$X^2\Sigma^+$	
0		0.9667	0.0317
1	0.0333	0.9034	0.0586
2	0.0648	0.8450	0.0813
3	0.0945	0.7910	0.1002
4	0.1230	0.7411	0.1158
5	0.1498	0.6950	0.1285
6	0.1753	0.6524	0.1385
7	0.1994	0.6131	0.1463
8	0.2224	0.5768	0.1520
9	0.2442	0.5432	0.1559

DETERMINATION OF INTERNAL STATE DISTRIBUTIONS

The detection method employed in these experiments measures the number density of a reaction product rather than the flux. Since product populations are

proportional to flux, we must consider the laboratory velocity $\mathbf{v}_{LAB}$ of the recoiling product, which factor relates flux to number density. In particular, we must consider the possible variation of average lab. velocities for products formed with different internal energies. In these experiments where no angular distribution measurements have been attempted, we are interested in obtaining the total flux associated with a specified set of internal states, e.g., one vibrational level. Thus populations refer to total cross sections (detailed rate constants) for formation of this specified set.

Fig. 7 shows Newton diagrams for reactions (1)-(4). The concentric circles centered on the tip of the centre of mass velocity vector $\mathbf{v}_{CM}$ indicate the magnitudes of the BaX recoil speeds for various internal energies. Reaction exoergicities are calculated using BaX dissociation energies estimated by Gole, Jonah and Zare [20] and HX dissociation energies from Darwent.[21] It is clear that for all possible internal energies $\mathbf{v}_{LAB}$ lies close to $\mathbf{v}_{CM}$. Indeed, in the worst case, Ba + HI, $\mathbf{v}_{LAB}$ differs from $\mathbf{v}_{CM}$ by a maximum of ± 15 %, and the typical difference is expected to be much less. This situation is well-known to be unfavourable to conventional angular distribution studies [3]; however, it facilitates the analysis of this experiment since we are justified in assuming that the magnitude and angular distribution of $\mathbf{v}_{LAB}$ is the same for each internal state, and hence no correction is necessary to relate measured number density to population.

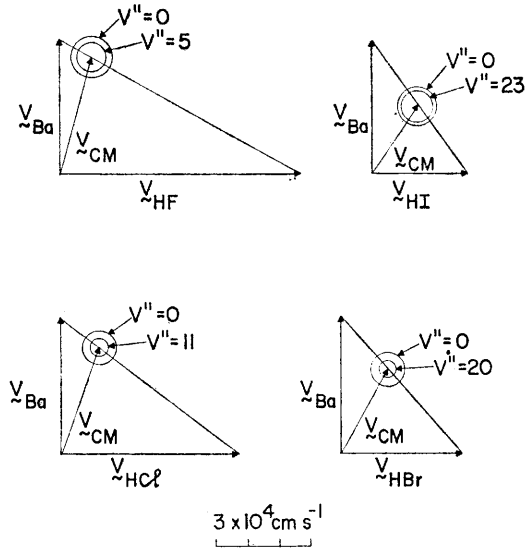

FIG. 7.—Newton diagrams for the Ba + HX reactions. Most probable velocities are used. The Ba beam is assumed to be effusive, while for the supersonic HX beam it is assumed that $\frac{1}{2}mv_{HX}^2 = \frac{5}{2}kT_0$, where T_0 is the upstream temperature. The concentric circles show the range of BaX speeds corresponding to the range of observed vibrational states v''. (In the text, $\underset{\sim}{V}$ is printed as $\mathbf{v}$).

The principal information determined from the fluorescence spectra is the values of vibrational band intensities $I_{v'v''}$ (energy s^{-1}). These are related to vibrational populations $N_{v''}$ by

$$I_{v'v''} = k[N_{v''}\rho(\lambda_{v'v''})q_{v'v''}] \sum_{v} v_{v'v}^4 q_{v'v} S(\lambda_{v'v}) \qquad (2)$$

where $\rho(\lambda_{v'v''})$ is the laser power density (energy cm^{-3}) at the wavelength of the (v', v'') band, q is a Franck–Condon factor for the transition designated by the subscripts,

$S(\lambda_{v'v})$ is the phototube sensitivity at the wavelength of the (v', v) band, $\nu_{v'v}$ is the frequency of the same band and k is a proportionality constant that includes parameters such as geometrical factors and the electronic transition moment (assumed to be constant). The term in brackets in eqn (2) represents the absorption process, while the summation represents the subsequent fluorescence pathways (assumed to occur only to the ground state) terminating in the various vibrational levels v.

The application of eqn (2) assumes that $I_{v'v''}$ is linearly proportional to $\rho(\lambda_{v'v''})$. This is valid in the limit of no radiation trapping and no optical pumping [22] of the molecular sample. Under our experimental conditions, the former poses no problem, whereas the latter requires consideration because of the high laser intensity used. Indeed, we observe a departure from linearity, which decreases as the laser intensity is reduced. Data, such as that shown in fig. 3-6, are taken with the laser intensity attenuated by typically fourfold, at which condition the deviation from linearity is $\sim$15 %. To simplify data analysis, the same laser intensity (to within 20 %) is used for all scans, and only linear corrections to $I_{v'v''}$ are made for variation in laser intensity.

(*a*) Ba + HF → BaF + H

The $\Delta v = 0$ sequence of the $C^2\Pi_{\frac{1}{2}}$–$X^2\Sigma^+$ band system is used to obtain the vibrational state populations of BaF since the band heads (formed by the $Q_1 + R_{12}$ branches) are well separated (see fig. 3). The vibrational band intensities are taken to be proportional to the areas of these heads above the weaker " background " formed by other headless branches. This procedure should be valid because (1) it is known from the spectroscopic constants in table 1 that $Q_1 + R_{12}$ lines with N'' values $\leqslant$150 fall within 0.1 nm of the head ($N''_{\text{head}} \approx 40$) and (2) the populations of high N'' levels are

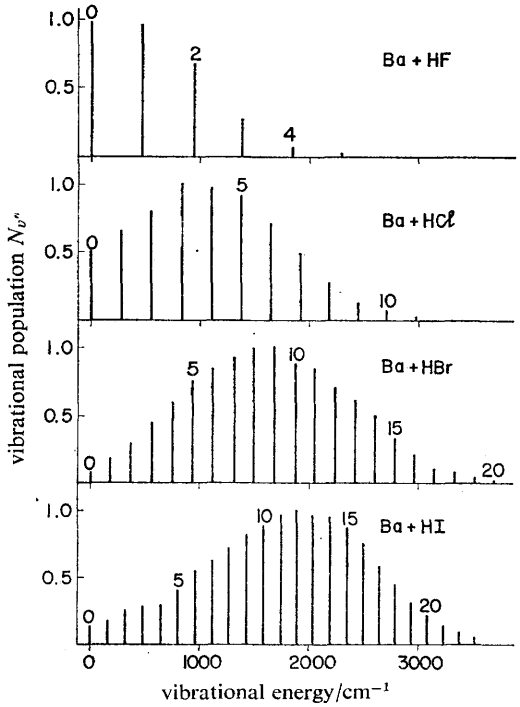

FIG. 8.—Relative vibrational populations for the reactions Ba + HX.

small since the R_1 heads, which would occur at 499.3 nm for the (0, 0) band, 499.6 nm for the (1, 1) band, etc., are not formed ($N''_{head} \approx 119$). Hence, fluorescence from all significantly populated rotational levels is included in the measured band head intensities. The vibrational populations are listed in table 3 and displayed in fig. 8.

TABLE 3.—VIBRATIONAL POPULATIONS $N_{v''}$ FOR THE Ba+HX REACTIONS [a]

v''	$N_{v''}$(BaF)	$N_{v''}$(BaCl)	$N_{v''}$(BaBr) [b]	$N_{v''}$(BaI)
0	(1.00)	0.51	0.09	0.16
1	0.97	0.66	0.19	0.19
2	0.68	0.80	0.30	0.26
3	0.28	(1.00)	0.46	0.29
4	0.06	0.98	0.59	0.29
5	0.01	0.91	0.76	0.41
6		0.72	0.85	0.55
7		0.49	0.92	0.63
8		0.26	1.00	0.71
9		0.12	(1.00)	0.81
10		0.05	0.90	0.89
11		0.02	0.84	0.97
12			0.70	(1.00)
13			0.60	0.97
14			0.49	0.96
15			0.32	0.87
16			0.21	0.76
17			0.12	0.59
18			0.07	0.45
19			0.04	0.32
20			0.02	0.23
21				0.16
22				0.09
23				0.06

[a] The populations are normalized to the most probable level, indicated by parentheses. The estimated errors in $N_{v''}$ for BaF and BaCl are ± 5 % for the most highly populated levels; for BaI and BaBr the errors are larger, perhaps ± 10 % (excluding the unknown systematic error in the $q_{v'v''}$ for BaBr).

[b] Data for the $\Delta v = 0$ sequence, see text.

While individual rotational lines are not observed, it is still possible to estimate the $v'' = 0$ rotational distribution from the envelope of the (0, 0) band R_1 branch in the region 499.3 to 499.6 nm, which is not overlapped by other branches. The intensity $I(\lambda)$ at a wavelength λ is given by

$$I(\lambda) = k' N_{N''} S(N'') / [|\mathrm{d}\nu/\mathrm{d}N''|(2J''+1)] \qquad (3)$$

where $N_{N''}$ is the population and $S(N'')$ is the line strength [23] of the R_1 branch of the rotational level $N'' = J'' - \frac{1}{2}$, $[\mathrm{d}\nu/\mathrm{d}N'']^{-1}$ expresses the variation of the number of rotational lines per unit frequency and k' is a proportionality constant. Since no R_1 head is observed, the N'' values greater than N''_{head} make a negligible contribution to $I(\lambda)$. For the N'' levels in the isolated region, $50 \leqslant N'' \leqslant 110$, a fit to a rotational temperature $T_{rot} = 800 \pm 100$ K is obtained.

We have attempted to simulate the observed fluorescence spectrum using the determined vibrational populations and various rotational distributions. A calculated spectrum is convoluted with the measured laser bandwidth profile and compared with the experimental scans to determine the " best " rotational distribution. We

find that if all vibrational states are assumed to have the same T_{rot}, the value of about 800 K provides the best fit. Moreover, it is found that several other distribution functions cannot reproduce the experimental spectrum; these functions include (1) $N_{N''}$ = constant for $N'' \leqslant N_{cutoff}$ (step function), (2) $N_{N''} = (2N''+1)$ for $N'' \leqslant N_{cutoff}$ (linear ramp), (3) $N_{N''} = 1 - N''/N_{cutoff}$ for $N'' \leqslant N_{cutoff}$ (negative linear ramp), and (4) $N_{N''} = \exp(-N''/K)$ (exponential). We conclude that the most probable N'' value of the experimental distribution must lie close to N''_{head} of the $Q_1 + R_{12}$ branch. The convolution procedure also provides a check on the method for determining band intensities. It is found that the band head areas of the computer-synthesized spectra ($T_{rot} \approx 800$ K) agree with the input vibrational populations to 2 %.

(*b*) Ba + HCl → BaCl + H

The BaCl $C^2\Pi_{\frac{3}{2}}$–$X^2\Sigma^+$ $\Delta v = 0$ and -1 sequences are well resolved (fig. 4) and are used for analysis. Vibrational band intensities are again estimated from areas of the band heads above a " background "; and populations, determined using the Franck–Condon factors in table 2, are shown in fig. 9*a* for the two sequences. The agreement of the $N_{v''}$ values deduced from the two sequences is encouraging, as it is a sensitive test of the consistency of the analysis. Because the $\Delta v = 0$ sequence is the more intense and because its Franck–Condon factors are expected to be more reliable, we present in table 3 and fig. 8 the $N_{v''}$ values from the $\Delta v = 0$ sequence.

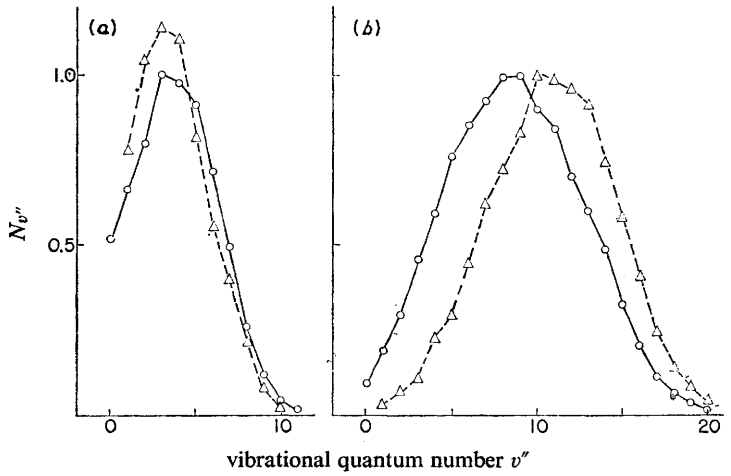

FIG. 9.—Relative vibrational populations derived from different sequences: solid line, $\Delta v = 0$ sequence; dashed line, $\Delta v = -1$ sequence. (*a*) The Ba + HCl reaction using the Franck–Condon factors given in table 2. Here the data are normalized so that the total population is equal for both sequences. (*b*) The Ba + HBr reaction assuming constant Franck–Condon factors in a sequence. Here the data are normalized so that for the most probable v'', $N_{v''}$ equals unity.

A rough estimate of the rotational distribution can be obtained in the same manner as for BaF. A rotational temperature of 1000 K, independent of vibrational level, appears to be consistent with the observed fluorescence spectrum. The band head areas of the computer-synthesized spectra agree with the input data to 10 % for the stronger bands.

The reaction Ba + DCl has also been studied. The population distributions for both vibration and rotation are very similar to the Ba + HCl results.

(*c*) Ba + HBr → BaBr + H

The $\Delta v = 0$ and -1 sequences of the $C^2\Pi_{\frac{1}{2}}$–$X^2\Sigma^+$ subband of BaBr are moderately well resolved (see fig. 5), but the $\Delta v = 0$ sequence comprises only 45 % of the total intensity of the subband. Because Franck–Condon factors are not available, the conversion of vibrational band intensities to vibrational populations is impeded. An attempt to extract $N_{v''}$ is made by assuming that the Franck–Condon factors in a sequence are constant. The results for the $\Delta v = 0$ and -1 sequences are shown in fig. 9*b*. Since the Franck–Condon factors are expected to decrease with v'' in the $\Delta v = 0$ sequence but increase with v'' in the $\Delta v = -1$ sequence (see table 2), the actual vibrational population distribution is expected to be intermediate between those given in fig. 9*b*. We have chosen to present in table 3 and fig. 8 the values of $N_{v''}$ as deduced from the $\Delta v = 0$ band intensities with the above assumption.

(*d*) Ba + HI → BaI + H

In the BaI C–X band system, the $\Delta v = 0$ sequence in each subband comprises about 95 % of the total intensity. Accordingly, we are well justified in assuming $q_{v'v''} = \delta_{v'v''}$. Table 3 and fig. 8 present the values of $N_{v''}$ as deduced from the $\Delta v = 0$ sequence of the $C^2\Pi_{\frac{1}{2}}$–$X^2\Sigma^+$ subband. This subband proved preferable because of the large variation of laser intensity over the $C^2\Pi_{\frac{1}{2}}$–$X^2\Sigma^+$ $\Delta v = 0$ sequence.

(*e*) RELATIVE TOTAL REACTIVE CROSS SECTIONS

For each reaction, the fluorescence from all bands of the BaX C–X system has been measured in order to estimate the relative total reactive cross sections σ_r. The ratio of the electronic transition moments, the factor in the proportionality constant k in eqn (2) needed to relate different molecules, is obtained from the estimated radiative lifetimes of the C states.[7] The σ_r are estimated using both the scattering chamber and

TABLE 4.—FRACTIONAL ENERGY DISPOSAL AND RELATIVE CROSS SECTIONS

reaction	exoergicity [a]/ eV	E_V/eV	E_R/eV	$\bar{f}_V$	$\bar{f}_R$	$\bar{f}_T$	σ_r [b] scatt. chamber	σ_r [b] crossed beams
Ba + HF	0.55	0.06	0.07	0.12	0.13	0.75	0.12	
Ba + HCl	0.48	0.13	0.09	0.28	0.18	0.54	0.60	0.28
Ba + DCl	0.42	0.12	0.09	0.29	0.20	0.51	0.40	0.14
Ba + HBr	0.61	0.22 [c]		0.36			(1.00)	(1.00)
Ba + HI	1.26	0.22		0.18			0.67	0.41

[a] Taken as $D_0^\circ(\mathrm{BaX}) - D_0^\circ(\mathrm{HX}) + E + W$, where D_0° is the dissociation energy, E is the relative collision energy (using the most probable speeds, see fig. 7) and W is the reactant internal excitation energy. [b] The cross sections are normalized to the Ba + HBr reaction. [c] Average for the $\Delta v = 0$ and -1 sequences (see fig. 9*b*).

crossed beam arrangements. In the former, an ionization gauge is used to measure HX pressure, and no correction for the change in gauge calibration for different gases has been made. In the crossed-beam experiments, it is assumed that the beam densities for the different HX reactants are equal when the upstream nozzle pressures are the same. HX upstream pressures p_0 of <20 Torr are used, under which conditions the fluorescence signals are linearly proportional to p_0. Pressures of HCl, DCl, HBr, and HI are measured with a stainless steel Bourdon gauge (Matheson). No data have been taken for HF since a suitable pressure gauge was not available. Results are presented in table 4.

DISCUSSION

LASER-INDUCED FLUORESCENCE AS A MOLECULAR BEAM DETECTOR

The technique of laser-induced fluorescence as set forth in this Discussion is applicable to many molecules and reaction systems, whose number will increase as the wavelength range of tunable lasers is extended. Although this technique would encounter the same difficulties as conventional molecular beam methods in determining angular distributions for kinematically unfavourable reactions, nevertheless it is possible to obtain information on the translational energy of the products from a knowledge of the internal state distribution and the reaction exoergicity. This is demonstrated here for the reactions Ba+HX.

The laser source that we have used is capable of exciting a high percentage (> 10 %) of molecules absorbing at the laser wavelength and present in the observation zone during the pulse. However, since the laser pulse rate (10 pps) is less than the rate at which molecules are replenished in the observation zone ($\sim 5 \times 10^4$ s^{-1}), only a small percentage of the total product flux is sampled. The laser pulse rate could ideally be increased to match the replenishment rate. Lasers with pulse rates on the order of 10^3 pps are presently available. Alternatively c.w. dye lasers can be used with similar gains in detection efficiency. The present detection system could be further improved by increasing the light collection efficiency (10^{-3}) by perhaps a factor of 10. With the present arrangement it has been possible to detect a density of 5×10^4 molecule cm^{-3} of BaO in an individual (v'', J'') level for the reaction [4] $Ba + O_2 \rightarrow BaO + O$, corresponding to an absorbance of only 10^{-8}. The potential sensitivity of the laser-induced fluorescence technique promises to make feasible the measurement of the angular distribution of a product in an individual (v'', J'') state and conceivably the velocity distribution as well by measurement of the absorption line Doppler profile.

THE Ba+HX REACTIONS

Table 4 summarizes the results for these reactions, where $\bar{E}_V$ and $\bar{E}_R$ denote the average BaX vibrational and rotational energies and $\bar{f}_V$, $\bar{f}_R$ and $\bar{f}_T$ denote the fractions of the total reaction exoergicity that appear as vibration, rotation and translation, respectively. The Ba+HX reactions are characterised by little vibrational and rotational excitation of the products, and there is a positive correlation of $\bar{f}_V$ with σ_r. We also note that the cross section for the reaction Ba+DCl is only ~60 % of that for Ba+HCl. A similar result has been obtained for the K+HBr and K+DBr reactions.[24]

In general, it appears that exothermic reactions lead to the efficient formation of vibrationally excited products. This is expected for attractive reaction surfaces, in which most of the energy is released as the reactants approach. Trajectory calculations on repulsive surfaces, in which only a small amount of energy is released as the reactants approach, also show in general that a large fraction of the reaction exoergicity appears as vibrational excitation (mixed energy release).[25] However, for the exothermic Ba+HX reactions, the average product vibrational excitation does not exceed 36 % and in the case of Ba+HF is only 12 %. This suggests that these reactions proceed on highly repulsive surfaces where mixed energy release plays little role.

It is plausible that the variation in σ_r in this homologous series of reactions is caused by the existence of a barrier along the reaction coordinate, the barrier height being negatively correlated with σ_r. Mok and Polanyi [26] have found using LEPS surfaces and the BEBO method that as the barrier height decreases, the location of the

barrier occurs earlier along the reaction coordinate. They have further found that earlier barrier locations lead to increased release of energy into vibrational excitation of the products. Thus, the positive correlation between σ_r and $\bar{f}_v$ observed in these reactions is consistent with the existence of a variable-height barrier. However, it is interesting to note that the Ba+HCl and Ba+DCl reactions, which proceed on the same potential energy surface and hence have the same barrier height, yield approximately equal $\bar{f}_v$ but different σ_r.

From fig. 8, it is seen that the shapes of the vibrational distributions are smooth and decidedly non-thermal in character. In the case of BaCl, BaBr and BaI, there is definate vibrational population inversion. The rotational distributions are less well characterized but the BaF distribution appears to be described quite satisfactorily by a temperature.

Hofacker and Levine [27] have proposed a non-adiabatic model in which the product vibrational distributions are described by a single parameter g, taken as a measure of the attractive character of the potential energy surface.[28] In this model, $g^2/2$ is equal to $\bar{E}_v/\hbar c\omega_e$. We find that the BaX vibrational distributions are fit moderately well to the functional form given by Hofacker and Levine and that the parameter g increases monotonically along the series. Such a model shows promise as a means of relating the details of the product internal state distribution to the potential energy surface of the reaction.

We thank R. R. Herm, R. D. Levine, and J. C. Polanyi for helpful correspondence, and we are grateful to A. Schultz for his contributions to the construction of the experimental apparatus. This work has been supported by the U.S. Air Force Office of Scientific Research under Grant AFOSR-72-2275 and by the U.S. Office of Naval Research under Contract N00014-67-A-0108-0035.

[1] J. L. Kinsey, *Molecular Beam Reactions*, in *International Review of Science: Reaction Kinetics* (MTP, Oxford, 1972).
[2] D. H. Maylotte, J. C. Polanyi and K. B. Woodall, *J. Chem. Phys.*, 1972, **57**, 1547, and references therein.
[3] C. A. Mims, S.-M. Lin and R. R. Herm, *J. Chem. Phys.*, 1972, **57**, 3099.
[4] A. Schultz, H. W. Cruse and R. N. Zare, *J. Chem. Phys.*, 1972, **57**, 1354.
[5] T. R. Dyke, B. J. Howard and W. Klemperer, *J. Chem. Phys.*, 1972, **56**, 2442.
[6] T. W. Hänsch, *Appl. Opt.*, 1972, **11**, 895.
[7] P. J. Dagdigian, H. W. Cruse and R. N. Zare, *J. Chem. Phys.*, 1974.
[8] F. A. Jenkins and A. Harvey, *Phys. Rev.*, 1932, **39**, 922.
[9] A. E. Parker, *Phys. Rev.*, 1934, **46**, 301. The vibrational assignment of the R_2+Q_{21} band heads (denoted by Q_2 by Parker) of the $\Delta v = -1$ sequence is erroneous. The vibrational quantum numbers should be reduced by one.
[10] K. Hedfeld, *Z. Phys.*, 1931, **68**, 610.
[11] R. E. Harrington, *Ph.D. Thesis* (University of California, 1942).
[12] P. Mesnage, *Ann. Phys.* (Paris), 1939, **11** (12), 5.
[13] With the exception of the $A^2\Pi_i$ state of BeF, all known A parameters of the $^2\Pi$ states of the alkaline earth monohalides are positive. See T. E. H. Walker and W. G. Richards, *J. Phys. B*, 1970, **3**, 271.
[14] See G. Herzberg, *Spectra of Diatomic Molecules* (Van Nostrand, Princeton, N.J., 1950), p. 261, for the line positions of the branches of a $^2\Pi(a)$–$^2\Sigma^+$ system.
[15] Ref. (14), pp. 101 ff.
[16] R. F. Barrow, M. W. Bastin and B. Longborough, *Proc. Phys. Soc.*, 1967, **92**, 518.
[17] P. A. Akishin, V. P. Spiridonov, G. A. Sobolev and V. A. Naumov, *Zhur. Fiz. Khim.*, 1958, **32**, 58.
[18] E. Morgan and R. F. Barrow, *Nature*, 1960, **185**, 754.
[19] B. R. K. Reddy and P. T. Rao, *J. Phys. B*, 1970, **3**, 1008. The vibrational assignment of the first entry in their table 1 is erroneous, and this band was omitted from the fit.

[20] J. L. Gole, C. D. Jonah and R. N. Zare, unpublished results.
[21] B. de B. Darwent, *Bond Dissociation Energies in Simple Molecules*, NSRDS-NBS 31 (U.S. Government Printing Office, 1970).
[22] R. E. Drullinger and R. N. Zare, *J. Chem. Phys.*, 1969, **51**, 5532.
[23] See R. N. Zare, *Rotational Line Strengths: The* O_2^+ $b^4\Sigma_g^- - a^4\Pi_u$ *Band System* in *Molecular Spectroscopy: Modern Research*, K. N. Rao and C. W. Mathews, eds. (Academic Press, New York, 1972).
[24] (*a*) K. T. Gillen, C. Riley and R. B. Bernstein, *J. Chem. Phys.*, 1969, **50**, 4019; (*b*) J. R. Airey, E. F. Greene, K. Kodera, G. P. Peck and J. Ross, *J. Chem. Phys.*, 1967, **46**, 3287.
[25] J. C. Polanyi, *Acc. Chem. Res.*, 1972, **5**, 161; B. A. Hodgson and J. C. Polanyi, *J. Chem. Phys.*, 1971, **55**, 4745.
[26] M. H. Mok and J. C. Polanyi, *J. Chem. Phys.*, 1969, **51**, 1451.
[27] G. L. Hofacker and R. D. Levine, *Chem. Phys. Letters*, 1971, **9**, 617.
[28] (*a*) R. D. Levine, *Chem. Phys. Letters*, 1971, **10**, 510; (*b*) G. L. Hofacker and R. D. Levine, *Chem. Phys. Letters*, 1972, **15**, 165.

Note added in proof: The exoergicities listed in column 2 of table 4 were calculated using the following value of D_0°(BaX): 6.33 eV for BaF, 4.84 eV for BaCl, 4.28 eV for BaBr, and 4.22 eV for BaI. These values of D_0°(BaX) were based on the preliminary analysis of the chemiluminescence data of Gole *et al.*[20] We have listed these values to facilitate any corrections which may be necessary when accurate dissociation energies are known.